Article

Naturally Occurring Isorhamnetin Glycosides as Potential Agents Against Influenza Viruses: Antiviral and Molecular Docking Studies

Andrey Bogoyavlenskiy,* Irina Zaitseva, Pavel Alexyuk, Madina Alexyuk, Elmira Omirtaeva, Adolat Manakbayeva, Yergali Moldakhanov, Elmira Anarkulova, Anar Imangazy, Vladimir Berezin, Dmitry Korulkin, Aso Hameed Hasan, Mahmoud Noamaan, and Joazaizulfazli Jamalis

Read Online

ACCESS | Metrics & More | Article Recommendations | SI Supporting Information

ABSTRACT: Influenza remains one of the most widespread infections, causing an annual illness in adults and children. Therefore, the search for new antiviral drugs is one of the priorities of practical health care. Eight isorhamnetin glycosides were purified from Persicaria species, characterized by nuclear magnetic resonance spectroscopy and mass spectrometry and then evaluated as potential agents against influenza virus. A comprehensive in vitro and in vivo assessment of the compounds revealed that compound 5 displayed the most potent inhibitory activity with an EC_{50} value of 1.2−1.3 μM, better than standard drugs (isorhamnetin 28.0−56.0 μM and oseltamivir 1.3−9.1 μM). Molecular docking results also revealed that compound 5 has the lowest binding energy (−10.7 kcal/mol) among the tested compounds and isorhamnetin (−8.1 kcal/mol). The ability of the isorhamnetin glycosides to suppress the reproduction of the influenza virus was studied on a model of a cell culture and chicken embryos. The ability of active compounds to influence the structure of the virion, as well as the activity of hemagglutinin and neuraminidase, has been demonstrated. Compound 1, 5, and 6 demonstrated the most effective inhibition of virus replication for all tested viruses. Molecular dynamics simulation techniques were run for 100 ns for compound 5 with two protein receptors Hem (1RUY) and Neu (3BEQ). These results revealed that the Hem-complex system acquired a relatively more stable conformation and even better descriptors than the other Neu-complex studied systems, suggesting that it can be an effective inhibiting drug toward hemagglutinin than neuraminidase inhibition. Based on the reported results, compound 5 can be a good candidate to be evaluated for effectiveness in preclinical testing.
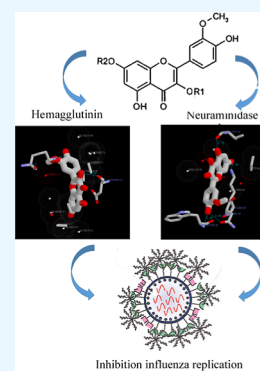
1. INTRODUCTION

Influenza A virus infections are a primary cause of acute respiratory viral infections and lead to substantial morbidity and mortality.[1,2] Despite the fact that vaccination is the main strategy against the influenza virus, a number of obstacles hinder its annual use, associated not only with insufficient effectiveness in children and older people but also with the long production time, which creates a high cost.[3−5] Therefore, the search for new antivirals is becoming increasingly important in the chemotherapy of viral infections. Despite significant progress in the search for drugs that can suppress the replication of the influenza virus at different stages of reproduction, only three groups of drugs are used in healthcare. The three categories of anti-influenza drugs are as follows: the neuraminidase (NA) inhibitors such as oseltamivir (Tamiflu)[6−10] and zanamivir[11] that have been approved in many countries worldwide, peramivir[12−15] and laninamivir[16−18] are approved in Japan. Peramivir is also approved in China and the Republic of Korea.[19] In addition, the M2 proton channel inhibitors amantadine and its derivative rimantadine stop the infection immediately after their administration.[20−23] The third group of compounds is a cap-dependent endonuclease inhibitor targeting the PA polymerase subunit (baloxavir).[24−26]

The emergence of influenza virus mutations capable of bypassing the action of these drugs has led to the need to continue the search for new compounds that can suppress the reproduction of the virus. One of the directions of such research is the search for pharmacologically active compounds isolated from plants.[27−29] Among the various classes of antiviral compounds of plant origin, the chemically diverse group of flavonoids is a prime target for research and individual flavonoid compounds have been assessed for the safety of regular intake and antiviral activity in vitro and in vivo.[30−32] It has been shown that a number of flavonoid aglycones have a pronounced ability to suppress the reproduction of various viruses in vitro and in vivo experiments, affecting various stages of their replication.[33−40] One such aglycone is isorhamnetin,[41−43] which occurs in plants in various glycosylated forms. Since glycosylation increases solubility, it is able to increase antiviral properties.

Table 1. Isorhamnetin Glycosides

Name	methoxyflavonol	Structure
Compound 1	Isorhamnetin 3-O-(3″-acetyl)-β-D-glucopyranoside	
Compound 2	Isorhamnetin 3-O-β-D-glucopyranosyl-(6→1)-(2‴,4‴-diacetyl)-α-L- rhamnopyranoside	
Compound 3	Isorhamnetin 3-O-(3″-acetyl)-β-D-glucopyranosyl-(6→1)-O-α-L-rhamnopyranoside	
Compound 4	Isorhamnetin 3-O-β-D- glucopyranosyl-(6→1)-(2‴,4‴-diacetyl)-α-L-rhamnopyranosyl-7-O-β-D-glucopyranoside	
Compound 5	Isorhamnetin 3-O-(3″-acetyl)-β-D-glucopyranosyl-(6→1)-O-α-L-rhamnopyranosyl-7-O-α-L-rhamnopyranoside	
Compound 6	Isorhamnetin 3-O-(2″-galloyl)-β-D-glucopyranoside	
Compound 7	Isorhamnetin 3-O-(2″-galloyl)-β-D-glucopyranosyl-7-O-α-L-rhamnopyranoside	
Compound 8	Isorhamnetin 3-O-(2″,6″-digalloyl)-β-D-glucopyranosyl-7-O-α-L-rhamnopyranoside	

Table 2. Inhibition of Virus Replication by Isorhamnetin Glycosides on the Model of MDCK[a]

compound	CC_{50}	A/Vladivostok/2/09 (H1N1)		A/Almaty/8/98(H3N2)		A/Tern/South Africa/1/61(H5N3)		A/chicken/FPV/Rostock/1934(H7N1)	
		EC_{50}	SI	EC_{50}	SI	EC_{50}	SI	EC_{50}	SI
compound 1	>192.3	32.7 ± 0.075	**>5.9**	18.5 ± 0.084	**>10.4**	24.0 ± 0.35	**>8.0**	23.5 ± 0.13	**>8.2**
compound 2	>141.2	197.7 ± 0.7	>0.7	190.7 ± 0.67	>0.7	70.6 ± 0.76	>2.0	98.9 ± 0.54	>1.4
compound 3	>150.2	285.3 ± 0.72	>0.5	180 ± 0.78	>0.8	135.1 ± 0.67	>1.1	51.2 ± 0.47	>2.93
compound 4	>114.9	109.2 ± 0.92	>1.1	126.4 ± 0.63	>0.9	218.4 ± 0.79	>0.5	155.2 ± 0.8	>0.7
compound 5	>123.2	1.3 ± 0.04	**>98.0**	1.2 ± 0.021	**>100.0**	1.3 ± 0.025	**>95.2**	1.3 ± 0.019	**>93.5**
compound 6	>158.7	14.9 ± 0.07	**>10.6**	2.2 ± 0.024	**>71.4**	2.5 ± 0.019	**>62.5**	2.7 ± 0.026	**>58.8**
compound 7	>133.0	259.3 ± 0.68	>0.5	252.7 ± 0.74	>0.5	166.2 ± 0.76	>0.8	219.4 ± 0.84	>0.6
compound 8	>107.8	129.3 ± 0.8	>0.8	97.0 ± 0.53	>1.1	161.6 ± 0.57	>0.7	188.6 ± 0.54	>0.6
isorhamnetin	>280.0	56.0 ± 0.45	**>5.0**	28.0 ± 0.34	**>10.0**	35.4 ± 0.18	**>7.9**	34.6 ± 0.43	**>8.1**
oseltamivir	>100.0	9.091 ± 0.04	**>11**	1.33 ± 0.028	**>75.0**	1.65 ± 0.027	**>60.06**	2.0 ± 0.025	**>50.0**

[a]CC_{50}, cytotoxicity/FCE concentration for 50% of cells; EC_{50}, effective antiviral concentration for 50% of virus; SI, selectivity index, CC_{50} [μM]/EC_{50} [μM]. Selective index values above 3[44,45] across all four tested viruses are highlighted in bold.

Table 3. Inhibition of Virus Replication by Isorhamnetin Glycosides on the Model of FCE[a]

compound	CC_{50}	A/Vladivostok/2/09 (H1N1)		A/Almaty/8/98(H3N2)		A/Tern/South Africa/1/61(H5N3)		A/chicken/FPV/Rostock/1934(H7N1)	
		EC_{50}	SI	EC_{50}	SI	EC_{50}	SI	EC_{50}	SI
compound 1	>288.3	32.7 ± 0.075	**>8.8**	18.5 ± 0.084	**>16.0**	24.0 ± 0.35	**>12.0**	23.5 ± 0.13	**>12.5**
compound 2	>211.8	197.7 ± 0.7	>1.1	190.7 ± 0.67	>1.1	70.6 ± 0.76	>3.0	98.9 ± 0.54	>2.13
compound 3	>225.3	285.3 ± 0.72	>0.78	180 ± 0.78	>1.25	135.1 ± 0.67	>1.67	51.2 ± 0.47	>4.4
compound 4	>184.8	109.2 ± 0.92	>1.69	126.4 ± 0.63	>1.46	218.4 ± 0.79	>0.85	155.2 ± 0.8	>1.18
compound 5	>185.8	1.3 ± 0.04	**>142.9**	1.2 ± 0.021	**>150.4**	1.3 ± 0.025	**>142.3**	1.3 ± 0.019	**>142.3**
compound 6	>158.7	14.9 ± 0.07	**>10.6**	2.2 ± 0.024	**>71.8**	2.5 ± 0.019	**>63.5**	2.7 ± 0.026	**>58.8**
compound 7	>238.0	259.3 ± 0.68	>1.24	252.7 ± 0.74	>0.95	166.2 ± 0.76	>1.43	219.4 ± 0.84	>1.1
compound 8	>161.7	129.3 ± 0.8	>1.25	97.0 ± 0.53	>1.65	161.6 ± 0.57	>0.95	188.6 ± 0.54	>0.85
isorhamnetin	>420.0	56.0 ± 0.45	**>75.0**	28.0 ± 0.34	**>15**	35.4 ± 0.18	**>12.0**	34.6 ± 0.43	**>12.1**
oseltamivir	>150.0	9091 ± 0.04	**>16.67**	1.33 ± 0.028	**>112.8**	1.65 ± 0.027	**>90.9**	2.0 ± 0.025	**>75.0**

[a]CC_{50}, cytotoxicity/FCE concentration for 50% of cells; EC_{50}, effective antiviral concentration for 50% of virus; SI, selectivity index, CC_{50} [μM]/EC_{50} [μM]. Selective index values above 3[44,45] across all four tested viruses are highlighted in bold.

This article describes the effect of isorhamnetin glycosylation on the inhibition replication influenza in cell lines and embryonated eggs.

2. RESULTS

Eight isorhamnetin glycosides obtained from plants in the genus Persicaria were purified and analyzed by spectroscopy to confirm purity and resolve their chemical structure (Tables 1 and S1). The analytes were classified as isorhamnetin glycosides with a unique combination of additional chemical groups in addition to the central flavonoid structure consisting of two phenyl rings and one heterocyclic ring. Acidic hydrolysis of compound 1 and compound 6 resulted in the cleavage of glucose and the formation of unsubstituted isorhamnetin. Phasic acidic hydrolysis of compounds 1−5 and compounds 7−8 resulted in the consistent cleavage of rhamnose and glucose with the formation of unsubstituted isorhamnetin. Alkaline hydrolysis of compounds 6−8 resulted in the cleavage of gallic acid from substances. The alkaline melt of all substances (compounds 1−8) gave a product as 1,3,5-trioxybenzol and 3-methoxy-4-oxybenzoic acid. In our studies, all isorhamnetin glycosides contained at least one additional carbohydrate group (Tables 1 and S1).

2.1. Antiviral Potency of the Isorhamnetin Glycosides. The main goal of this study was to identify the isorhamnetin glycoside (Table 1) with the lowest cytotoxicity and the highest antiviral activity among the tested flavonoids.

We investigated the influence of isorhamnetin glycoside treatment on the cell viability of MDCK cells and fertilized chicken eggs (FCEs). The isorhamnetin glycosides did not produce significant cytotoxic effects in the MDCK cells or FCEs (Tables 2 and 3). For the antiviral screening, we infected the cells and FCEs with the influenza virus and determined the antiviral potency of each flavonoid.

It was shown that isorhamnetin glycosides had different SI index values (Tables 2 and 3). CC_{50} values for isorhamnetin glycosides were 107−280 and 158−420 μM in FCEs (Tables 2 and 3). While several isorhamnetin glycosides showed minor antiviral activity against a single, multiple, or all tested viruses, compound 5 and compound 6 resulted in a marked reduction in virus replication in cells for all tested viruses (Tables 2 and 3). Compound 1 was more efficient in reducing virus replication at high doses. Compound 2 only showed a marginal reduction in virus titers. Compound 3, a molecule similar to compound 2, inhibited the replication of H3N2 and H7N1 efficiently at the highest concentration. For compound 4, at all concentrations and all viruses, only a minor reduction in virus replication was observed. Compound 5 resulted in an almost complete block in replication for all tested viruses. Compound 6 displayed a dose-dependent increase in antiviral activity. Compound 7 and 8 isorhamnetin glycosides did not show antiviral activity for all tested influenza viruses. Oseltamivir, a licensed NA inhibitor, and isorhamnetin were used as references in our assays.

Table 4. Functional Inhibitory Assays[a]

compound	A/Vladivostok/2/09 (H1N1)	A/Almaty/8/98(H3N2)	A/Tern/South Africa/1/61 (H5N3)	A/chicken/FPV/Rostock/1934 (H7N1)
		Virus Titer Reduction Factor (VTRF)		
compound 1	1.5 ± 0.02	1.5 ± 0.05	2.0 ± 0.01	1.5 ± 0.03
compound 5	3.0 ± 0.01	2.8 ± 0.04	4.1 ± 0.07	3.0 ± 0.05
compound 6	1.0 ± 0.05	1.0 ± 0.05	1.0 ± 0.05	1.0 ± 0.04
isorhamnetin	1.5 ± 0.02	1.5 ± 0.02	1.9 ± 0.02	1.5 ± 0.02
oseltamivir	1.0 ± 0.02	1.0 ± 0.02	1.0 ± 0.01	1.0 ± 0.02
		Hemagglutination Inhibition Concentration 50 (HIC_{50} μM)		
compound 1	157.0 ± 2.1	52.9 ± 0.5	40.8 ± 0.5	47.0 ± 1.6
compound 5	151.5 ± 3.0	37.0 ± 1.0	27.3 ± 0.63	97.4 ± 2.7
compound 6	184.8 ± 5.5	176.4 ± 2.7	191.3 ± 1.54	188.5 ± 3.8
isorhamnetin	156.3 ± 2.0	50.5 ± 0.45	39.3 ± 0.7	48.2 ± 1.7
oseltamivir	154.8 ± 5.1	144.8 ± 6.6	154.8 ± 2.0	134.8 ± 6.6
		Neuraminidase Inhibition Concentration 50 (NIC_{50} μM)		
compound 1	70.5 ± 2.1	130 ± 4.1	380.4 ± 8.8	66.3 ± 1.4
compound 5	17.4 ± 0.4	14.4 ± 0.4	22.7 ± 0.5	14.5 ± 0.5
compound 6	45.6 ± 1.6	39.4 ± 1.2	3.3	37.5 ± 1.1
isorhamnetin	68.3 ± 1.8	125 ± 4.0	370 ± 7.5	68.2 ± 1.2
oseltamivir	6.0 ± 0.32	4.0 ± 0.2	20.3 ± 0.5	6.1 ± 0.2

[a]Reduction factors were calculated based on the difference in the EID_{50} titers and were classified as slight (RF 1−2), moderate (RF 2−3), and strong (RF ≥ 3) virucidal activity. Compound 1 had slight virucidal activity against different types of influenza. A strong virucidal effect on all viruses in the panel was observed for Compound 5. Compound 6 had slight virucidal activity against viruses in the test panel.

Suppression of viral replication was dose-dependent, and complete absence of viral replication was observed at micromolar concentrations equal to or lower than those of oseltamivir and isorhamnetin (Table 3). For subsequent studies, the three most effective glycosides (compound 1, compound 5, and compound 6) with SI values greater than or comparable to oseltamivir and isorhamnetin were selected.

2.2. Influence of Isorhamnetin Glycosides on the Virus Yield Reduction Assay. In order to characterize the mechanism through which isorhamnetin produces anti-influenza effects, we carried out the virucidal activity or virus titer reduction factor (VTRF) of the isorhamnetin glycosides in the panel was assessed in ovo (Table 4).

2.3. Inhibitory Effect of Isorhamnetin Glycosides on the Hemagglutination and Neuraminidase Activity. The inhibitory capacity of isorhamnetin glycosides on the hemagglutination and NA activity of panel viruses toward chicken erythrocytes was assessed from a starting concentration of 1 μM (Table 4). Compound 1 and compound 5 were able to inhibit hemagglutination of any tested virus. Compound 5 has the largest effect on all viruses tested with the minimum HIC_{50} for H5N3 (27.3 μM), and the maximum HIC_{50} against the H1N1 influenza virus (151.5 μM). The effect of isorhamnetin glycosides on the activity of the NA protein of our panel of viruses was determined in a NA inhibition assay (Table 4). Compound 1 inhibited the NA activity of any virus in our assay from the concentration up to 66.3−380.4 μM. Compounds 5 and 6 inhibited the NA activity in our assay at concentrations 14.4−22.7, 37.5−88.9 versus 4.0−20.3 μM for oseltamivir. These results suggest that isorhamnetin glycosides may produce additional inhibitory effects on virus replication via virus adsorption on cells and virion release by the inhibition of NA.

2.4. Molecular Docking. Molecular docking of three isorhamnetin glycosides on the model of influenza virus hemagglutinin and NA (Tables 5 and S2−S5) showed that the studied preparations have more activity than isorhamnetin.

Table 5. Binding Energy of the Selected Ligands with Those of the Studied Proteins

no.	compound	ligand binding energy (kcal/mol) to influenza hemagglutinin (1RUY)		ligand binding energy (kcal/mol) to influenza NA (3BEQ)	
		affinity (kcal/mol) max	affinity (kcal/mol) min	affinity (kcal/mol) max	affinity (kcal/mol) min
1	compound 1	−8.7	−8.3	−7.5	−6.9
2	compound 5	−10.7	−9.6	−8.8	−7.8
3	compound 6	−9.6	−8.9	−8.7	−7.8
4	isorhamnetin	−8.1	−7.4	−7.8	−7.0

They have a high probability of suppressing the activity of influenza virus hemagglutinin and NA since they are able to form additional hydrogen bonds with the amino acid residues of the active centers of the studied proteins. At the same time, if on the hemagglutinin model, these compounds form one group that binds amino acids involved in the formation of the hemagglutinin binding site, then on the NA model, these compounds form two groups. Thus, compound 1 inhibits the site of enzyme activity, while compound 5 and compound 6 block the formation of the enzyme's tertiary complex.

2.4.1. In Silico Predicted the ADMET Parameters of the Isorhamnetin Glycosides. In this study, in-silico predictions were made for the physicochemical and ADMET parameters of the compounds under investigation, as shown in Table 6. The obtained results were then compared to the optimal range of drug−likeness parameters, which has been adhered to by 95% of marketed drugs.[79,80] Of particular interest were two parameters: log P and half-life (see Table 7).

The octanol/water partition coefficient (log P) is a parameter used in drug discovery to assess how a drug molecule distributes between lipid and aqueous environments. It quantifies a compound's hydrophobicity or its affinity for fats versus water. The log P value is determined experimentally by comparing the concentrations of a compound in octanol and water. A positive log P value indicates higher solubility in

Table 6. In Silico Predicted the ADMET Parameters of the Isorhamnetin Glycosides

molecular property	value				unit
	isorhamnetin	compound 1	compound 5	compound 6	
absorption	prediction	prediction	prediction	prediction	
caco-2 permeability	−5.18	−5.55	−5.67	−5.64	log(cm/s)
aqueous solubility (log P)	2.291	−2.366	−1.325	0.746	log(mol/L)
oral bioavailability	42.37	39.16	40.9	38.39	%
distribution	prediction	prediction	prediction	prediction	
BBB	19.67	14.34	19.4	15.09	%
PPBR	34.07	36.77	38.69	37.38	%
VDss	2.96	2.84	3.62	3.41	L/kg
excretion	prediction	prediction	prediction	prediction	
half-life	54.63	114.73	120.22	115.93	h
toxicity	prediction	prediction	prediction	prediction	
ames	42.33	41.34	42.51	40.54	%
LD_{50}	1.85	1.81	2.3	2.09	−log(mol/kg)

(a) Hem   **(b) Neu**
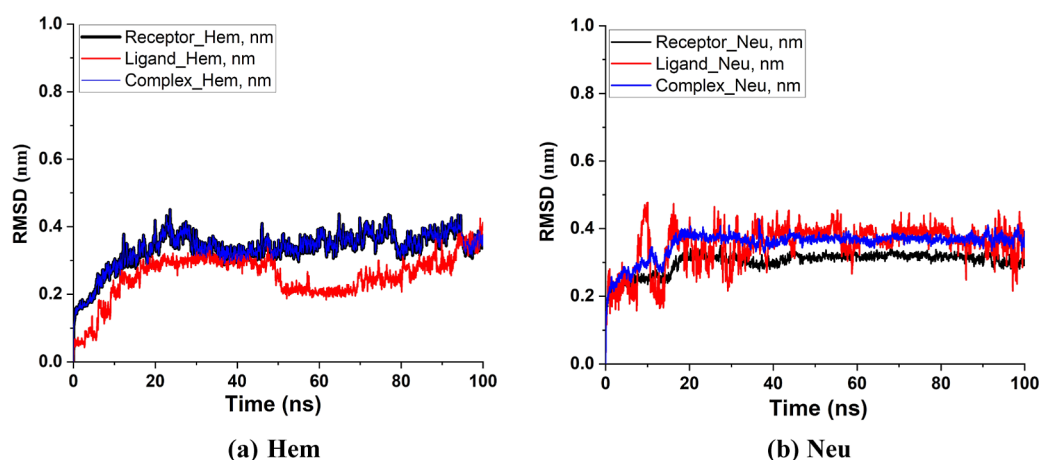
Figure 1. RMSD of solvated ligand, receptor, and protein complexes (Hem and Neu) during 100 ns MD simulation time.

octanol, suggesting that the compound is more lipophilic, while a negative value suggests higher solubility in water, indicating greater hydrophilicity. The log P value is important for predicting a drug's absorption, distribution, and overall pharmacokinetic behavior. Compounds with moderate log P values are typically preferred for optimal drug perform-ance.[79,80] Among the four compounds, three compounds (1, 3, and 4) met the recommended optimum value for log P.

Prediction of the toxicity of the investigated isorhamnetin glycosides showed that the investigated drugs have a higher rate of penetration through intestinal tissue. Compounds have less ability to penetrate the blood−brain barrier and lower toxicity (Table 6). A distinctive feature of the studied compounds is their higher half-life, which provides a more pronounced therapeutic effect.

2.5. Molecular Dynamics Simulation and System Stability. The molecular interactions and the water solvent conditions around the protein influence the conformational stability of the protein−ligand interaction. The best-docked (Compound 5) pose with the highest binding affinity with two protein receptors (Hem and Neu) was utilized as the starting structure. Also, its interaction and stability were predicted using a molecular dynamics simulation.[13,14] Therefore, a long-range MD simulation of 100 ns was performed on docked complexes in order to investigate the dynamics, conformational stability, and structural stability of the protein−ligand complex.

The stability of the systems was measured in this study using the root-mean-square deviation (RMSD) during the 100 ns simulations versus the first frame. The most acceptable RMSD value range was <5.0 Å, as the lower RMSD value indicates superior stability of the system.[5] For all frames of the protein receptors (Hem or Neu), the ligand (Compound 5) and ligand−protein complex systems are presented in Figure 1 a and b. In the case of Hem complex, the average RMSD values were 3.354, 2.550, and 3.375 Å; meanwhile, in the Neu complex, the values were 3.414, 3.519, and 3.554 Å, respectively. The standard deviation of the average RMSD values were 0.528, 0.658, and 0.533 Å in the case of Hem complex; meanwhile, in the Neu complex, the values were 0.408, 0.662, and 0.391 Å, respectively.

2.6. Binding Free Energies. A popular method for determining accurately the binding free energies of receptor− vaccine complexes is the molecular mechanics energy technique (MM-GBSA and -PBSA). GBSA combines the generalized Born and surface area continuum solvation model, while the one-average molecular mechanics Poisson−Boltz-mann surface area (MM-PBSA) approach[12,15,16] is path independent which is used to calculate the binding free energy by analyzing ensembles of the initial and final state; thus, the efficiency of MM-PBSA is better than MM-GBSA. Both techniques may be more reliable, less computationally expensive, and more productive than docking scores.[17] The binding free energies of the simulated complexes were

Table 7. Summary of the Binding Free Energy of MM-PBSA and MM-GBSA Calculated for Solvated Protein Complexes (Hem and Neu) During 100 ns MD Simulation Time, and All Values Are Given in (kcal/mol)[a]

	ΔV_{DWAALS}			GBSA			
				ΔE_{GB}	$\Delta E_{SURF}/\Delta E_{NPOLAR}$	ΔG_{SOLV}	ΔT_{OTAL}
Hem	−49.14	−53.27	−102.42	84.05	−7.87	76.18	**−26.23**
					PBSA		
				93.03	−6.57	86.47	**−15.95**
Neu	−20.06	−21.05	−41.11	32.12	−2.99	29.13	**−11.98**
					PBSA		
				31.38	−2.54	28.85	**−12.26**

[a] ΔE_{VDW} = van der Waals energy; ΔE_{ELE} = electrostatic energy; ΔG_{GAS} = gas-phase free energy; ΔG_{sol} = solvation free energy; ΔE_{SURF} = surface energy; ΔE_{GB} = generalized Born energy; ΔE_{PB} = Poisson−Boltzmann energy; ΔE_{NPolar} = nonpolar energy; ΔG_{bin} = calculated total binding free energy (kcal/mol). MM-GBSA = molecular mechanics-generalized Born surface area; MM-PBSA = molecular mechanics Poisson−Boltzmann surface area.

computed based on the molecular dynamics (MD) simulation results to revalidate the protein affinity predicted by docking simulation studies for receptor−ligand complexes. All reported computed contribution of each energy term in MM-GBSA and MM-PBSA for both complexes is tabulated in Table 1. High negative values indicate beneficial interactions and high receptor−ligand affinity, while positive net binding energy demonstrates low-docked stability. The net binding free energy of Hem complex was calculated to be −26.23 or −15.95 kcal/mol corresponding to GBSA and PBSA, respectively, and for the Neu complex, it was calculated to be −11.98 or −12.26 kcal/mol corresponding to GBSA and PBSA, respectively (see Table 7).

3. DISCUSSION

It is known that a number of flavonoid aglycones are capable of suppressing the replication of viruses, and glycosylation increases their biological properties.[32−43] In our studies, we conducted a comparative study of 8 isorhamnetin derivatives to suppress the reproduction of the influenza virus. Here, we report the molecular structure and antiviral activities of eight isorhamnetin glycosides that contain chemical groups in addition to the flavonoid aglycone. Purified extracts from plants of the Persicaria genus (eight molecules of isorhamnetin—O-methylated flavonoids, differing in carbohydrate fragments in positions 3-O and 7-O of the isorhamnetin aglycone molecule) were assessed for the effectiveness of suppressing the infectivity and replication of influenza A viruses (Table 1). All isorhamnetin glycosides in this study contained at least one additional carbohydrate group, but differed in size and location of the glycoside and the presence of gallic acid and acetyl groups.[30] Influenza A viruses (IAV) A/Vladivostok/2/09 (H1N1), A/Almaty/8/98 (H3N2), A/Tern/South Africa/1/61 (H5N3), and A/chicken/FPV/Rostock/1934 (H7N1) were chosen to represent both seasonal human and potentially zoonotic avian influenza A virus subtypes. As previous studies have found higher antiviral activity of the isorhamnetin aglycone over quercetin and kaempferol aglycones, we chose to characterize naturally occurring isorhamnetin glycosides as they contain additional reactogenic groups with potential antiviral effects.[40−60] Toxicity and efficiency of individual compounds were evaluated in MDCK and embryonated chicken eggs (Tables 2 and 3). All tested isorhamnetin glycosides displayed low toxicity in ovo. Combined with the fact that these substances have been used in traditional medicine for many decades, a rather favorable safety profile can be attributed to all isorhamnetin glycosides in this study. The

ratio of CC_{50} and EC_{50} concentrations is reported as a measure of the balance between the toxic effect and antiviral activity. Higher CC_{50}/EC_{50} values represent more active and safer compounds, whereas values close to or below 1 are considered less favorable. Isorhamnetin glycoside 1 (compound 1), a 3-O-glucopyranoside with a linked acetyl group, was efficient in reducing influenza virus replication at high doses, whereas compound 2, consisting of two glucose moieties and two acetyl groups bound to a rhamnose sugar in the isorhamnetin backbone, only showed a marginal reduction in virus titers. In contrast, flavonoid compound 3, a molecule similar to compound 2, but having only one acetyl group bound to the glucose moiety, inhibited the replication of H3N2 and H7N1 more effectively than H5N3 and H1N1. Only a minor reduction in virus replication was observed for flavonoid compound 4 at all concentrations and all viruses. This isorhamnetin glycoside, like compound 2, had a 3-O-glucose-diacetyl-rhamnose residue and an additional 7-O-glucose. Compound 5, an isorhamnetin molecule similar in size compared to compound 4 and a configuration of the glycoside moieties analogous to compound 3, but with an additional 7-O-rhamnopyranoside at the A ring of the isorhamnetin backbone, resulted in an almost complete block in replication for all tested viruses. Compound 6 harboring one galloyl group bound to the 3-O-glucose displayed a dose-dependent increase in anti-influenza activity. An additional 7-O-rhamnose moiety (compound 7) and a second galloyl residue (compound 8) in the structure of the isorhamnetin glycoside led to an almost complete loss in antiviral activity toward all IAVs. Taken together, these results suggest that the acetylated glycoside residue on the C ring at the 3-O position of the isorhamnetin molecule might determine anti-influenza A virus activity. To further decipher the mechanisms of the action of individual isorhamnetin glycosides corresponding to different stages during virus infection and replication, the following assays were employed: the determination of the virucidal activity prior to attachment to host cells, the inhibitory effect on the hemagglutinating activity of influenza A virus isolates involved in virus binding to extracellular receptors, and the inhibition of viral NA activity required for budding of newly formed virions. The ability to reduce the viral infectious titer was assessed at a concentration of 3 μM isorhamnetin glycoside (Table 4). Compound 1 and 6 had virus reduction factors comparable to those of oseltamivir (0.2−2.0 and 0.1−0.5, respectively), whereas preincubation with Compound 5 reduced viral titers at factors 2.8 to 4.1. Next, the reduction in hemagglutination activity of panel viruses toward chicken erythrocytes was
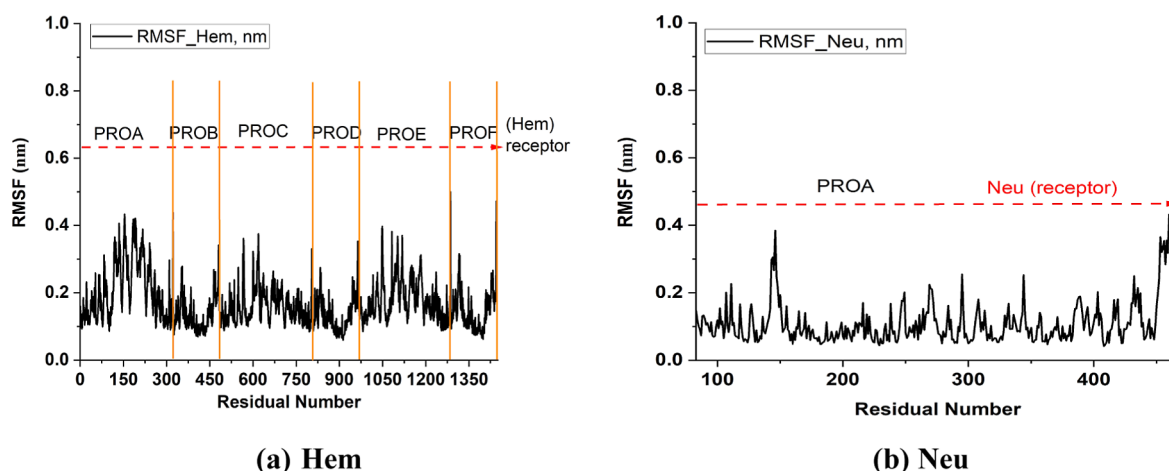
Figure 2. RMSF of solvated ligand, receptor, and protein complexes during 100 ns MD simulation time. (A) Hemagglutinin and (b) NA.

assessed. The hemagglutination inhibition (HI) assay represents a measure to quantify the compound's ability to reduce the binding of a virus to cell surface receptors and can thus roughly be interpreted as the capacity of the glycoside to prevent attachment of virions. Concentrations for the reduction of the hemagglutination titer of panel viruses were established at 40.8−157.0 μM for compound 1, 27.3−151.5 μM for compound 5, and 176.4−191.3 μM for compound 6 and all panel viruses. The effect of isorhamnetin glycosides on the NA activity of influenza viruses was determined via a NA inhibition assay. The inhibitory capacity of isorhamnetin glycosides on the activity of the virus's NA is found to be linked to the structure, number, and length of carbohydrate moieties, as well as the presence or absence of additional acetyl or galloyl groups. An acetylated glucose moiety at the 3-*O* position at the C ring of the isorhamnetin molecule is likely to be required for distinct NA inhibition properties.[40−43]

The evaluation of isorhamnetin glycosides on virus hemagglutination and NA activity revealed the effective inhibition of hemagglutination by the compounds for all tested viruses. The obtained results have practical implications, particularly in the context of virucidal activity prior to viral attachment to the host cells. The potent antiviral properties displayed by isorhamnetin glycosides raise the possibility of their application as disinfectants or biocides. Further research is warranted to explore their efficacy in practical settings and to evaluate their safety profiles. Such findings hold promise for the development of novel antiviral strategies and the potential utilization of isorhamnetin glycosides in combating viral infections outside the scope of traditional pharmaceutical interventions.

Molecular docking of compounds confirms that isorhamnetin glycosides are able not only to block the active sites of proteins but also to suppress the formation of quaternary complexes of viral proteins (Tables 5 and S2−S5).

Measurement of ADMET parameters showed greater safety of the studied compounds (Table 6).

Overall, the presented data enhance our understanding of structure−activity relationships with respect to the mechanism of virus-inhibitory actions of isorhamnetin glycosides. Compound 5, and to a lesser extent, compound 1 and compound 6 are the most promising newly described candidates leading to further preclinical evaluation since they display marked antiviral activity at several steps during the viral infection

and replication cycle and across several IAV subtypes. Concentrations of the tested isorhamnetin glycosides were in the low millimolar range and seemed suitable for the development of treatment regimens. Data on the bioavailability of flavonoid glycosides are sketchy and partially contradictory. One study reports peak titers in human plasma after the oral intake of quercetin glycosides within less than an hour, possibly allowing administration of the active compounds as an oral formulation during an acute viral infection.[52−57] Furthermore, studies have shown that glycosylated and methylated flavonoids are more lipophilic, and thus can be more readily transported through biological membranes, leading to increased cellular uptake over unglycosylated flavonoids.[58−60] Moreover, methylated and glycosylated flavonoids have high hepatic metabolic stability and high intestinal absorption in comparison with unmethylated and unglycosylated equivalents.[59,60]

The best-docked (compound 5) pose with the highest binding affinity with two protein receptors (Hem and Neu) was studied through molecular dynamics simulation. These results revealed that the Hem-complex system acquired a conformation relatively more stable than that of the other Neu-complex studied systems. The RMSD during the 100 ns simulations versus the frame of 0.1 (ns) time ago is also analyzed, as presented in Figure S1a,b, which gives the values as 1.113, 0.648, and 1.113 Å, in the case of Hem complex; meanwhile, in the Neu complex, the values were 0.946, 0.885, and 0.967 Å, respectively. By taking the composition of studied complexes into consideration, results revealed that the Hem-complex system acquired a relatively more stable conformation than the other Neu-complex studied systems.

Examining residue behavior and its relationship with the ligand during MD simulation production requires evaluating protein structural flexibility upon ligand binding.[18] Using the root-mean-square fluctuation (RMSF) method, protein residue variations were assessed to determine the impact of inhibitor binding to the relevant targets across 100 ns of simulations. The calculated average RMSF values for the Hem complex and Neu complex of protein systems were 1.676 and 1.115 Å, respectively. The standard deviation of the average RMSF values were 0.714 and 0.690 Å, respectively. Figure 2a,b depicts the overall residue fluctuations of both protein−ligand complex systems. The terminal residues in contrast to the core residues were found to have more fluctuations, which are expected due
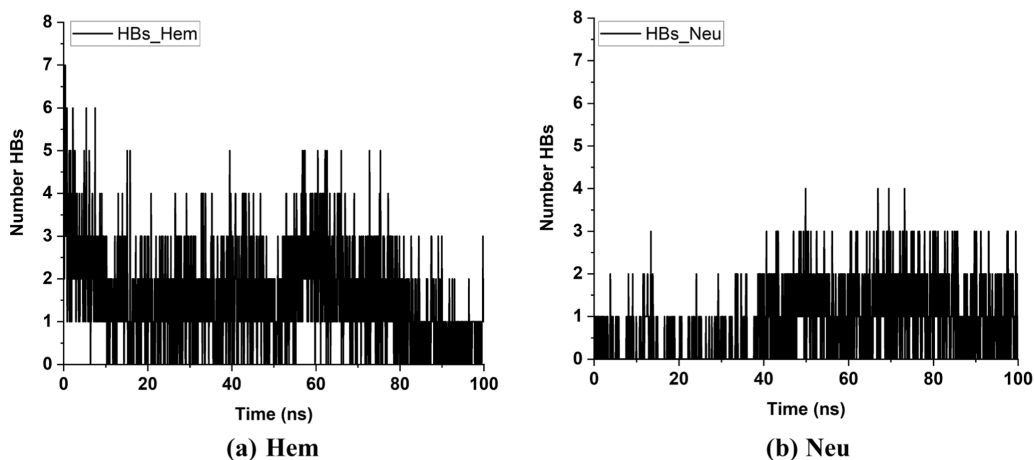
(a) Hem   **(b) Neu**

Figure 3. Number of average hydrogen-bonding interaction between the protein receptor and ligand in solvated protein complexes during 100 ns MD simulation time. (A) Hemagglutinin and (b) NA.
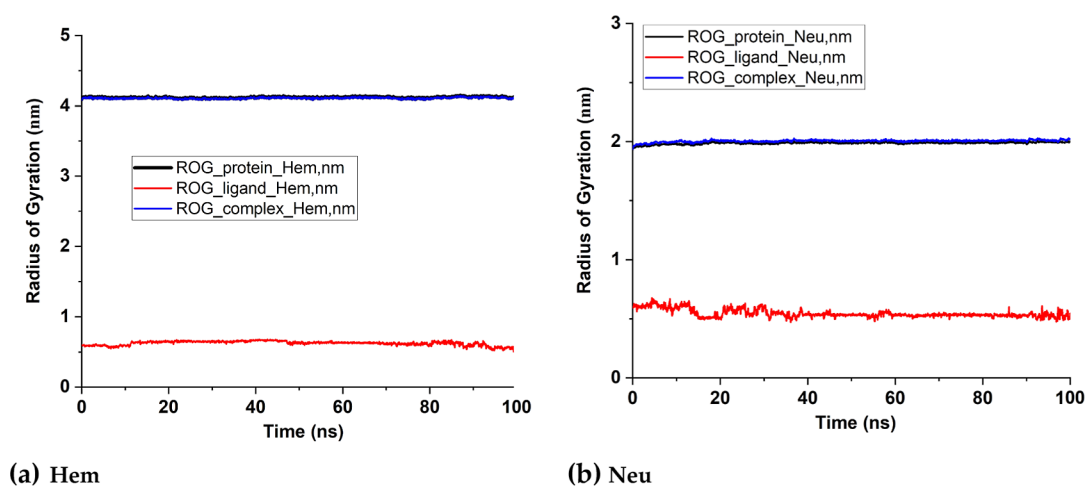

(a) Hem   **(b) Neu**

Figure 4. Radius of gyration (R_g) of solvated ligand, receptor, and protein complexes during 100 ns MD simulation time. (A) Hemagglutinin and (b) NA.
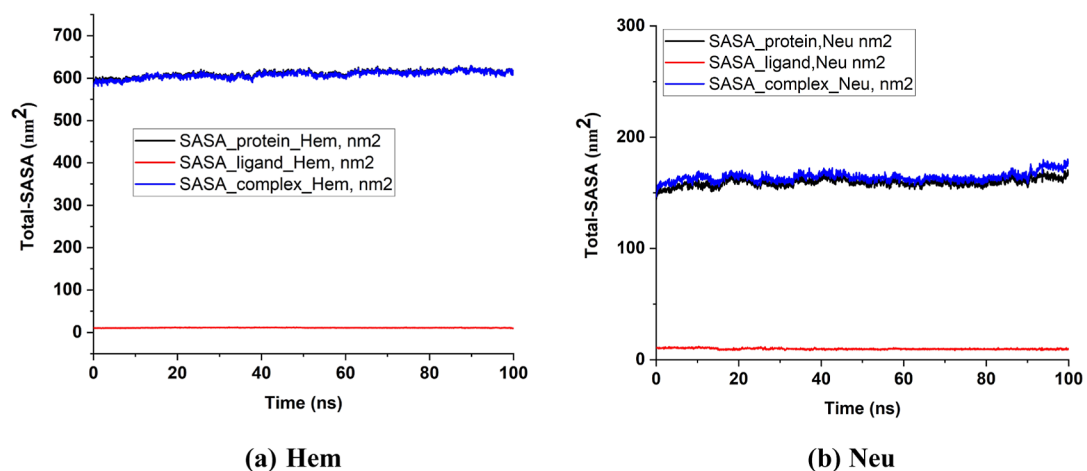

(a) Hem   **(b) Neu**

Figure 5. SASA analysis for solvated ligand, receptor, and protein complexes during 100 ns MD simulation time. (A) Hemagglutinin and (b) NA.

to the flexible nature of the biomolecule terminals. Overall, the average RMSF of the systems is <3 Å, which indicates formation of highly stable complexes and good affinity of the ligand molecule for the receptors, which will be reflected well on the complex stability.

The number of hydrogen bond interactions occurring between protein and ligands were calculated with an angle cut = 20°, rcut = 3.0 Å, and plotted against time 100 ns as shown in Figure 3a,b. Upon calculation of hydrogen bonds, the average number of hydrogen bonds per time frame was

observed to be 1.538 and 0.794 Å for Hem and Neu complexes, respectively. During overall analysis, it was found that the ligand−protein interaction significantly increased the number of hydrogen bonds from 1 to 7 HBs per trajectory analysis in the case of Hem complex and from 1 to 4 in the case of Neu-complex systems. These values demonstrate that the Hem-complex system acquired a relatively more stable conformation than the other Neu-complex system studied by hydrogen-bonding interaction.

The protein structural compactness and simulation stability are both indicated by the radius of gyration (R_g). For all frames of both protein receptors (Hem or Neu), ligand (compound 5), and ligand−protein complex systems as presented in Figure 4a,b, the average R_g values were 4.116, 0.624, and 4.108 nm, in the case of Hem complex; meanwhile, in the Neu complex, the values were 1.987, 0.546, and 2.013 nm, respectively. The standard deviation of the average R_g values were 0.925, 0.345, and 0.923 Å, in the case of Hem complex; meanwhile, in the Neu complex, the values were 0.093, 0.344, and 0.352 Å, respectively, which is obvious because of the heavy nature of biomolecular receptor complexes. Overall, the average R_g of both protein complexes indicates compact formation of highly stable complexes which will be reflected well upon both complex stabilities.

The solvent accessible surface area (SASA) of the protein was calculated during MD simulation in ligand-bound conditions due to the binding of ligand to the protein. For all frames of both protein receptors (Hem or Neu), ligand (compound 5), and ligand−protein complex systems as presented in Figure 5a,b, the average SASA values were 609.793, 11.145, and 607.868 nm^2, in the case of Hem complex; meanwhile, in the Neu complex, the values were 159.271, 9.829, and 164.039 nm^2, respectively. The standard deviation of the average SASA values were 15.465, 0.547, and 15.627 nm^2, in the case of Hem complex; meanwhile, in the Neu complex, the values were 3.526, 0.558, and 4.230 nm^2, respectively. The analysis indicates the folding states of protein and its stability upon the ligand-binding affinity which is obvious because of the heavy nature of the complex as findings in results with a slight change in protein and its complexes.

Figure 6 shows the average distance of the center of mass of receptor residue (Hem or Neu) and ligand (compound 5) throughout the 100 ns simulation. The Neu complex shows great distance compared with the Hem complex and are kept
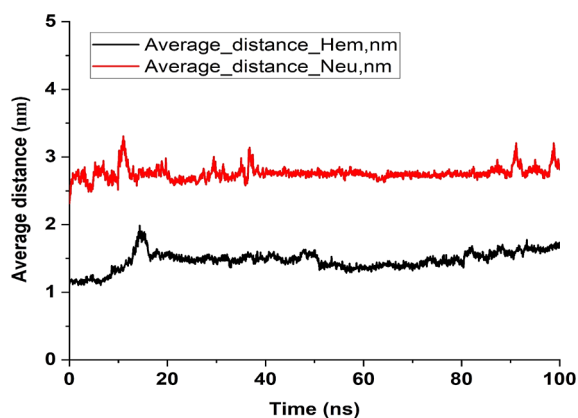
close to about 2.756 and 1.471 nm, respectively, as a function of time which reflects to the conformation stability of Hem complex other than the Neu complex.

To estimate the binding between the protein receptor (Hem or Neu) and the ligand (compound 5), a contact frequency (CF) analysis was performed utilizing the contactFreq.tcl module on VMD and with a cutoff of 4 Å as represented in Figure 7 a,b. In the simulated Neu-complex case study, the following amino acid residues exhibited higher CF values to 86.81%: MET187, TYR207, ASN208, ILE210, THR212, and LYS259. In the Hem complex, there are good contact surfaces with the protein pocket through the simulation study; the following amino acid residues exhibited higher CF values to 97.95%: PROA (LYS311), PROB (LYS575, ASN579, ASN582, LYS583, ASP586, GLY587, and ASP590), PROC (GLU107, GLN108, SER110, SER111, ARG262, SER264, GLY265, and SER266), and PROD (MET559, ASN560, THR561, GLN562, PHE563, and THR564) which indicate excellent binding affinity toward hemagglutinin than the NA inhibition complex.

A close inspection of the individual energy contributions reveals that the van der Waals energy and electrostatic energy, −49.14 (−53.27) and −20.06 (−21.05) kcal/mol, correspond to Hem and Neu complexes, respectively, where the van der Waals energy and electrostatic energy played a significant role in binding affinity for supporting the complex formation. Finally, surface and nonpolar component energies have considerable moderate values for complexes. The net binding free energy is ordered as Hem < Neu complex which leads to Hem complex finding the most stable conformation receptor−ligand affinity complex than the other Neu complex by 14.25 (3.69) kcal/mol corresponding to GBSA and PBSA, respectively, which is promising and has high affinity to ligand−receptor of hemagglutinin rather than NA and must be introduced to evaluate experimentally and to validate biological effectiveness of the designed drug construct.

4. MATERIALS AND METHODS

4.1. Cells, Virus, and Compounds. Madin−Darby canine kidney (MDCK) cells were obtained from the American Type Culture Collection and were routinely maintained using media recommended by the manufacturer.[61,62] The CPE of MDCK cells was expressed as 50% tissue culture infectious doses (TCID50), which were calculated based on the method of Reed and Muench.[63,64]

Ten day old FCEs were purchased from a licensed commercial vendor and incubated in a humidified incubator at 37 °C. All studies were carried out in accordance with local guidelines set up by the Ministry of Education and Science of the Republic of Kazakhstan and were approved by the Committee on Ethics of Animal Experiments at the Research and Production Center for Microbiology and Virology, Almaty, Kazakhstan (approval no. 02-12-18).

Oseltamivir-resistant human influenza A virus A/Vladivostok/2/09 (H1N1) was obtained from the virus collection of the Smorodintsev Research Institute of Influenza, St. Petersburg, Russia. Influenza virus A/Almaty/8/1998 (H3N2), a human seasonal influenza A virus strain, was obtained from the virus collection of the Research Institute for Biological Safety Problems, Gvardeyskiy, Kazakhstan. Highly pathogenic avian influenza viruses A/chicken/FPV/Rostock/1934 (H7N1) and A/Tern/South Africa/1/1961 (H5N3),
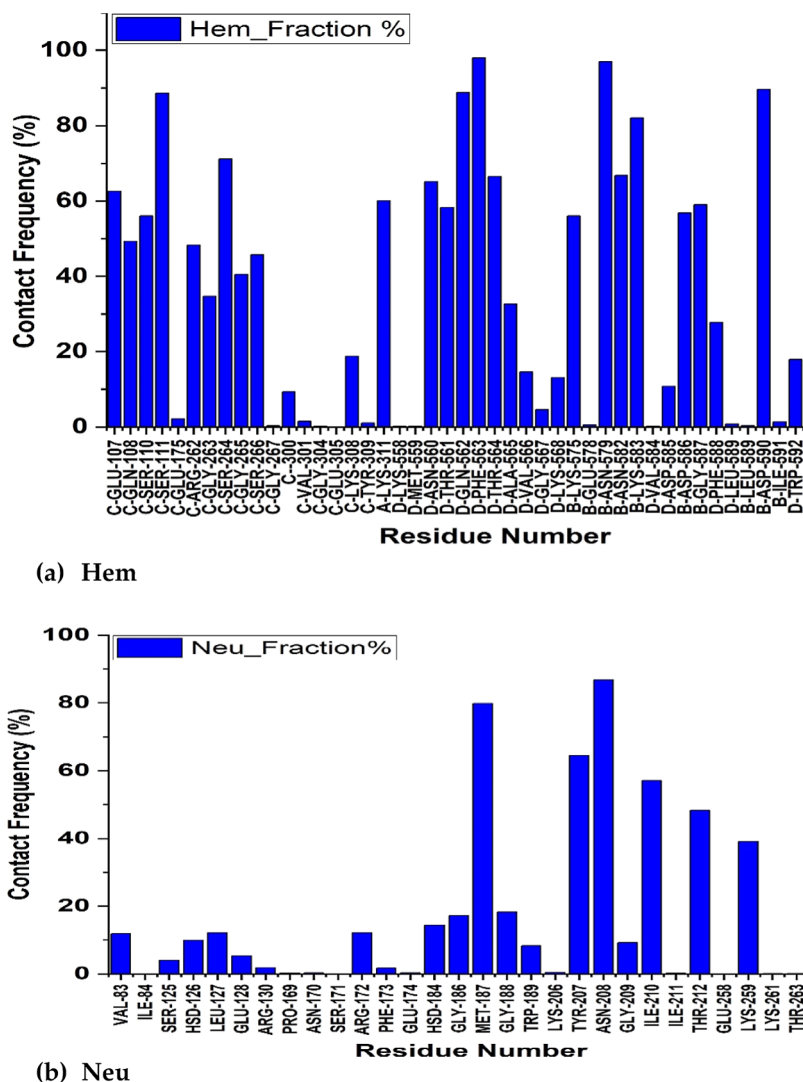

Figure 6. Average minimum distance between the ligand center versus the center of mass analysis of solvated protein complexes (Hem and Neu) during 100 ns MD simulation time.

Figure 7. CF percentage analysis for proteins−ligand complexes during 100 ns simulation time. (A) Hemagglutinin and (b) NA.

were obtained from the state collection of viruses at the Ivanovsky Institute of Virology, Moscow, Russia.

Tamiflu (Oseltamivir, 75 mg) was purchased from Roche Korea (Seoul, South Korea) Co. Ltd. When the dose of the drug was calculated, only the pure substance was taken into account.

4.2. Isorhamnetin Was Purchased from Sigma-Aldrich (USA).
Virus stock was titrated by scoring the cytopathic effect (CPE) microscopically on cells and hemagglutination assay on CFE and then, $TCID_{50}$ and EID_{50} were estimated using the Reed−Muench method.[63,64]

4.3. Origin of Plant Material.
Raw plant material from *Persicária maculósa* (*Polygonum* persicaria L) was purchased from an LCC "TES" (Kazakhstan, Almaty, Karasay Batyr Street, 128, license no. FD64605126R). A voucher specimen was obtained in the herbarium at the Institute of Botany and Phytointroduction of the Committee of Forestry and Wildlife of the Ministry of Ecology, Geology, and Natural Resources of the Republic of Kazakhstan (MHA0115410). The plant material after the removal of contaminants was crushed and dried for subsequent extraction. The authors declare that the experiments performed on the plants in this study comply with international and national guidelines.

4.4. Extraction and Spectral Analysis.
Isorhamnetin glycosides were extracted from milled, air-dried, raw plant material using 30% ethanol. To concentrate the flavonoids, the ethanol extract was heated to 50 °C under reduced pressure (Dehydrator Hurakan HKN-DHd32, China). The solution was fractionated with benzene and ethyl acetate (Sigma-Aldrich). Concentrated ethyl acetate extract was applied onto a Sephadex LH-20 (Sigma-Aldrich) dextran gel column and eluted in water and water−ethanol mixtures at increasing ratios (1:9 to 1:1). The separation of components was controlled by thin-layer chromatography on Silufol UV-254 plates (Kavalier, Czech Republic). The eluted fractions were combined, concentrated, and rechromatographed on silica gel columns using a mixture of chloroform and ethanol at increasing ethanol concentrations as eluent.[65] The purified compounds were then analyzed by high-performance liquid chromatography (HPLC) using 250 × 25 mm LiChrospher 60 RP 15 μm columns (Merck), 40 mL/min flow, and a mixture of methanol and H_2O at ratio 6:4.[65] Next, the chemical structure of individual compounds was determined by chemical analyses (phasic acid hydrolysis, alkaline hydrolysis, and alkaline melt) followed by spectral analysis (UV spectroscopy with complexing and ionizing additives, 13C-

nuclear magnetic resonance spectroscopy, and mass spectrometry). All purified compounds were obtained as amorphous powders and were dissolved in phosphate-buffered saline (PBS, pH 7.2, Invitrogen) for use in further experiments.

4.5. Toxicity of Isorhamnetin Glycosides in the MDCK Cell. To determine the 50% cytotoxic concentration (CC_{50}) for each of the tested isorhamnetin compounds, MDCK cells were seeded onto 96-well plates (NUNC, Penfield, NY, USA) at a density of 1×10^4 cells per well. MDCK cells were washed twice with PBS and the culture medium was replaced with a medium containing serially diluted flavonoids (concentrations from 10 μM up to 300 μM) for 48 h at 37 °C in a 5% CO_2 atmosphere. After incubation, the relative viable cell number was then determined by the MTT method.[66] In brief, the treated cells were incubated for another 3 h in a fresh culture medium containing 0.5 mg/mL MTT. Cells were then lysed with 0.1 mL of DMSO and the absorbance at 540 nm of the cell lysate was determined using a microplate reader (Infinite M200, Tecan Group Ltd. Switzerland). The CC_{50} was determined from the dose−response curve and the mean CC_{50} was calculated from three independent experiments.

4.6. Toxicity of Isorhamnetin Glycosides in Fertilized Chicken Eggs. Isorhamnetin glycoside dilutions were prepared at 25, 50, 100, 200, 400, and 800 μM in sterile PBS. 100 μL of each concentration was inoculated into the allantoic cavity of 10 day old FCEs. The eggs were incubated in a humidified incubator at 37 °C for 5 days, and viability was checked twice daily by candling. The 50% effective lethal dose (ELD_{50}), defined as the sample concentration resulting in 50% embryo survival, was calculated.

4.7. Antiviral Activity in MDCK Cells. Antiviral activity of the flavonoids against influenza infection was determined on MDCK cells infected with 100 TCID50 of the influenza virus (post-treatment method). Virus-induced cell death was measured using the MTT assay.[49] The effective concentration for 50% cell death (EC_{50}) was calculated. Finally, the in vitro anti-influenza virus activity of the flavonoid was expressed as SI (selective index, CC_{50}/EC_{50}), which is the value of CC_{50} (50% cytotoxic concentration) in MDCK cells divided by the value of EC_{50} (50% effective concentration) against influenza.[41,67−69]

4.8. Antiviral Activity in Embryonated Eggs. Various concentrations of the compounds were mixed with equal volumes of influenza virus at 100 EID_{50} and incubated for 30 min at 37 °C. After a 30 min incubation at 37 °C, the mixture was inoculated into the chorioallantoic cavity of 10 day old chicken embryos. The viruses were grown for 24−72 h at a temperature of 37 °C, depending on the virus strain. The presence of viruses was indicated by the hemagglutination test (HA test). The ability of the studied compounds to inhibit the infectious activity of the virus was assessed by comparing the results of the HA test in the experimental and control samples. As a control, instead of the test compounds, phosphate-buffered saline solution of pH 7.2 and the test virus were used.[63] The effective concentration of 50 for HA titers (EC_{50}) was calculated. The in vitro anti-influenza virus activity of the flavonoid was expressed as SI (selective index, CC_{50}/EC_{50}).[41,67−69]

4.9. Virucidal Activity. Equal volumes of the test virus and the investigated compound were mixed and incubated for 30 min at 37 C. The mixture was titrated into 10-fold dilutions and used for inoculation into the chorioallantoic cavity of 10 day old chicken embryos. After incubation for 24−72 h at 37 °C in a humidified incubator, EID_{50} was determined as

described by Reed and Muench.[64] Viral inocula treated with sterile phosphate buffer were used as a control for each virus. Infectivity suppression was expressed as the difference between log10 (EID_{50} treatment) and log10 (EID_{50} control). Three independent experiments with triplicate treatments were completed.

4.10. HI Assay. HI assay was used to determine the effect of extracts on virus adsorption as described earlier.[63]

4.11. NA Inhibition Assay. The NA activity was measured by a fluorometric assay with substrate 2′-(4-methylumbelliferyl)-α-d-N-acetylneuraminic acid according to the protocol of the Na-Fluor Influenza Neuraminidase Assay Kit (Applied Biosystems, Thermo Fisher Scientific). The fluorescence was measured using a microplate reader (Infinite M200, Tecan Group Ltd., Switzerland) at an excitation wavelength range of 350 to 365 nm and an emission wavelength range of 440 to 460 nm.[63]

4.12. Molecular Docking. Molecular modeling of the interaction of the analyzed compounds with the influenza proteins was carried out using a computer analysis of the activity of ligand binding to the target.[70,71] The ligand preparation was carried out in the PyMOL program 2.5.2 https://pymol.org/2/.[72−74] The computer simulation itself was carried out using AutoDock Vina program 1.1.2. http://vina.scripps.edu/, as well as some external tools, such as AutoDock Tools 1.5.6. http://mgltools.scripps.edu/downloads.[75,76] 2D visualization of the influenza proteins with a ligand was performed in the LigPlot + program 2.2.5 https://www.ebi.ac.uk/thornton-srv/software/LigPlus/download2.html.[77,78]

4.12.1. In Silico Prediction of ADMET Parameters. Prediction of ADMET properties isorhamnetin glycosides was carried out in silico with web server SwissADME https://ai-druglab.smu.edu/admet.[79−81] Several critical parameters were predicted to be log P, brain/blood partition coefficient (log BB), Caco-2 permeability (Caco-2), acute toxicity (Acute tox.), predicted LD_{50} (pLD_{50}), and Ames mutagenicity (Ames).

4.12.2. Computational Details. 4.12.2.1. Molecular Dynamics Simulation. The top consensus docking scores from target compound (compound 5) with receptors (Hem (1RUY) and Neu (3BEQ)) were advanced to all-atom MD simulations to study the relative stabilities of the protein−ligand interactions and screen the compound for further binding energy calculations. All simulations were done using the GROMACS V2022.4 package[82,83] and the CHARMM36[84] force field, the parameters and topological files for the selected compounds were generated using the latest CHARMM/CGenFF through CHARMM-GUI.[84,85] The protein−ligand complex was immersed at the center of a box of solvated water molecules with a TIP3P explicit solvation model, 0.15 M ions (410 Na^+ and 422 Cl^- in case of Hem complex, and 83 Na^+ and 78 Cl^- in case of Neu complex), to mimic the physiological salt concentrations, were added to provide charge neutralization and electrostatic screening which extended 20 Å from the protein.[6] CHARMM and the periodic boundary conditions were set with dimensions of a rectangular cubic system as 169.0, 169.0, and 169.0 Å in case of Hem complex, and 98.0, 98.0, and 98.0 Å in case of Neu complex in x, y, and z directions, respectively.[85]

The MD protocols involve minimization, equilibration, and production. No atoms were restrained in the 100 ns MD production simulations. The isothermal−isobaric (NPT)

ensemble and a 2 fs time integration step were chosen for all MD simulations. Through the 100 ns of MD production, the pressure was set at 1 atm using the Nosé−Hoover and Langevin piston barostats.[86,87] The temperature was set at 300.0 K using the Langevin thermostat.[88] For the minimization and equilibration of the complexes in the water box, we assumed force−field parameters excluding a scaling of 1.2 nm. All atoms, including those of hydrogen, were illustrated explicitly. Complex preliminary energy was minimized via 5000 steps at constant temperature (300 K), followed by the solvated protein−ligand complex system that was equilibrated with 500,000 steps and 50,000,000 runs for 100 ns. The structural coordinates were kept every 25 ps in the trajectories. The generated trajectories recovered from the production step were utilized for analysis of the whole system residues by using tools implemented in the GROMACS and VMD package.[89,90] A distance cutoff of the short-range neighbor list 1.0 nm was applied to short-range nonbonded interactions with a pair list distance of 1.2 nm, and Lennard-Jones interactions were smoothly truncated at 1.2 nm (rvdm, rcoulomb = 1.2 nm). Long-range electrostatic interactions were treated using the particle mesh Ewald (PME) method,[91] where a grid spacing of 1.0 Å was used for all simulation cells. For consistency, we applied the same protocol for all MD simulations.

4.12.2.2. Binding Energy Calculations. The binding free energy of the simulated complexes (Hem and Neu) were computed based on molecular dynamics (MD) simulation results by GROMACS using snapshots taken from the system's trajectories (100 ns) followed by gmx_MM-PBSA tool based on AMBER tools MM-PBSA.py module with GROMACS files[91−98] in which the ligand (L) binds to the protein receptor (R) to form the complex (RL). We are only interested in relative binding energy calculations, where the Gibbs relative binding energy is given by

$$\Delta G_{bind} = \Delta G_{bind,vacuum} + \Delta G_{RL,Solvation} - (\Delta G_R - \Delta G_L)$$

4.13. Statistical Analysis. Data are given as mean values with standard deviations from three independent experiments. To test the significance of differences, one-way analysis of variance (ANOVA) or a two-tailed Student's *t*-test was used. *P* values equal to or less than 0.05 were considered statistically significant.

5. CONCLUSIONS

In conclusion, our comprehensive analysis indicates that the presence of a balanced number of additional carbohydrate groups in isorhamnetin glycosides correlates with their high antiviral activity. These carbohydrate groups likely contribute to the overall molecular structure and spatial arrangement, enabling specific interactions with viral components that are crucial for viral infectivity and replication.

The stability of the systems was measured using RMSD during the 100 ns simulations. Obtained results revealed that the Hem-complex system acquired a relatively more stable conformation than the Neu complex. The calculated average RMSF values for the Hem complex and Neu complex to protein systems were 1.676 and 1.115 Å, respectively. The average number of hydrogen bonds per time frame was observed to be 1.538 and 0.794 Å for Hem more than Neu complexes, respectively. Average distance of the center of mass of receptor residues (Hem or Neu) and ligand (compound 5) were measured throughout the 100 ns simulation. The Neu

complex shows great distance compared with the Hem complex, which remains close to about 2.756 and 1.471 nm, respectively, as a function of time, which reflects the conformation stability of Hem complex compared to the other Neu complex.

The net binding free energy of the Hem complex was calculated to be −26.23 and −15.95 kcal/mol corresponding to GBSA and PBSA, respectively; whereas GBSA and PBSA values for the Neu complex were found to be −11.98 and −12.26 kcal/mol, respectively. The net binding free energy is ordered as Hem < Neu complex which leads to the Hem complex finding the most stable conformation receptor−ligand affinity complex more than the Neu complex by 14.25 (3.69) kcal/mol corresponding to GBSA and PBSA, respectively, which is promising and has high affinity to ligand−receptor of hemagglutinin rather than neuraminidase and must be introduced to evaluate experimentally and to validate biological effectiveness of the designed drug construct.

Moreover, the unsaturated hydroxyl positions within the carbon rings of isorhamnetin play a significant role in its antiviral properties. These unsaturated hydroxyl groups create additional intramolecular interactions, promoting structural flexibility and enhancing the compound's ability to target multiple viral mechanisms. By targeting different stages of the viral life cycle, such as viral entry, replication, and assembly, isorhamnetin glycosides exhibit a multifaceted approach to reduce virus infectivity and replication.

Isorhamnetin glycosides were tested against various viruses, showing different levels of antiviral activity. Among them, compounds 1, compound 5, and compound 6 demonstrated the most effective inhibition of virus replication for all tested viruses. These compounds were chosen for further studies due to their potency, comparable to that of reference antiviral compounds. The evaluation of isorhamnetin glycosides on virus hemagglutination and NA activity demonstrated that compounds 1 and 5 effectively inhibited hemagglutination for all tested viruses. Compound 5 showed the strongest effect with significant inhibition observed across multiple viruses. In addition, these compounds displayed inhibitory effects on NA activity, suggesting their potential to interfere with virus replication through viral attachment and virion release inhibition.

The presence of additional carbohydrate groups and unsaturated hydroxyl positions in isorhamnetin glycosides contributes to their ability to disrupt viral attachment and entry into the host cells. These compounds can competitively inhibit viral binding to cellular receptors, thereby preventing viral entry and subsequent infection. Additionally, the intricate structural features of isorhamnetin glycosides enable inter-actions with viral enzymes involved in replication, impairing viral genome replication, and transcription processes. Fur-thermore, these compounds may interfere with viral assembly and release, hindering the production of infectious viral particles.

Overall, our findings shed light on the molecular mechanisms underlying the antiviral activity of isorhamnetin glycosides. The balanced presence of additional carbohydrate groups and the unique unsaturated hydroxyl positions within the carbon rings contribute to the compound's broad-spectrum antiviral effects. The ability of isorhamnetin glycosides to target multiple stages of the viral life cycle suggests their potential as promising candidates for the development of novel antiviral therapeutics.

■ ASSOCIATED CONTENT

Data Availability Statement

All data generated or analyzed during this study are included in this published article and its Supporting Information.

ⓢ Supporting Information

The Supporting Information is available free of charge at https://pubs.acs.org/doi/10.1021/acsomega.3c08407.

> The following Supporting Information can be downloaded at www.mdpi.com/xxx/s1, structural characteristics of isorhamnetin glycosides, 3D visualization of ligand binding to the influenza hemagglutinin (1RUY) under study, 3D visualization of ligand binding to the influenza NA (3BEQ) under study, 2D visualization of ligand binding to the influenza hemagglutinin (1RUY) under study, 2D visualization of ligand binding to the influenza NA (3BEQ) under study, and root-mean-square deviation (RMSD) vs frame reference 0.1 ns ago of solvated ligand, receptor, and complexes of proteins (Hem and Neu) during 100 ns MD simulation (PDF)

■ AUTHOR INFORMATION

Corresponding Author

Andrey Bogoyavlenskiy − *Research and Production Center for Microbiology and Virology, Almaty 050010, Kazakhstan;* ⓞ orcid.org/0000-0001-9579-2298; Email: anpav_63@mail.ru

Authors

Irina Zaitseva − *Research and Production Center for Microbiology and Virology, Almaty 050010, Kazakhstan*

Pavel Alexyuk − *Research and Production Center for Microbiology and Virology, Almaty 050010, Kazakhstan*

Madina Alexyuk − *Research and Production Center for Microbiology and Virology, Almaty 050010, Kazakhstan*

Elmira Omirtaeva − *Research and Production Center for Microbiology and Virology, Almaty 050010, Kazakhstan*

Adolat Manakbayeva − *Research and Production Center for Microbiology and Virology, Almaty 050010, Kazakhstan*

Yergali Moldakhanov − *Research and Production Center for Microbiology and Virology, Almaty 050010, Kazakhstan*

Elmira Anarkulova − *Research and Production Center for Microbiology and Virology, Almaty 050010, Kazakhstan*

Anar Imangazy − *Research and Production Center for Microbiology and Virology, Almaty 050010, Kazakhstan*

Vladimir Berezin − *Research and Production Center for Microbiology and Virology, Almaty 050010, Kazakhstan*

Dmitry Korulkin − *Department of Chemistry and Chemical Technology, al-Farabi Kazakh National University, Almaty 050010, Kazakhstan*

Aso Hameed Hasan − *Department of Chemistry, College of Science, University of Garmian, Kalar, Kurdistan Region 46021, Iraq*

Mahmoud Noamaan − *Mathematics Department, Faculty of Science, Cairo University, Giza 12613, Egypt*

Joazaizulfazli Jamalis − *Department of Chemistry Faculty of Science, Universiti Teknologi Malaysia, UTM Johor Bahru, Johor 81310, Malaysia*

Complete contact information is available at:
https://pubs.acs.org/10.1021/acsomega.3c08407

Author Contributions

Pavel Alexyuk, Irina Zaitseva, Elmira Anarkulova, Anar Imangazy, Dmitry Korulkin, Aso Hameed Hasan, and Mahmoud Noamaan had full access to all of the data in the study and take responsibility for the integrity of the data and the accuracy of the data analysis. Concept and design: Andrey Bogoyavlenskiy, Madina Alexyuk, Elmira Omirtaeva, and Adolat Manakbayeva. Acquisition, analysis, or interpretation of data: Vladimir Berezin. Drafting of the manuscript: Andrey Bogoyavlenskiy and Joazaizulfazli Jamalis. Critical revision of the manuscript for important intellectual content: All authors. Statistical analysis: All authors.

Notes

Institutional Review Board Statement: "The animal study protocol was approved by the Ethics Committee of Research and Production Center for microbiology and virology (protocol code 02-12-39 from 22.07.2019)."
The authors declare no competing financial interest.

■ ACKNOWLEDGMENTS

■ REFERENCES

(1) Javanian, M.; Barary, M.; Ghebrehewet, S.; Koppolu, V.; Vasigala, V.; Ebrahimpour, S. A brief review of influenza virus infection. *J. Med. Virol.* **2021**, 93 (8), 4638−4646.

(2) Campolieti, M. Tail risks and infectious disease: Influenza mortality in the U.S., 1900−2018. *Infect. Dis. Model.* **2021**, 6, 1135−1143.

(3) Bhugra, P.; Grandhi, G. R.; Mszar, R.; Satish, P.; Singh, R.; Blaha, M.; Blankstein, R.; Virani, S. S.; Cainzos-Achirica, M.; Nasir, K. Determinants of Influenza Vaccine Uptake in Patients With Cardiovascular Disease and Strategies for Improvement. *J. Am. Heart Assoc.* **2021**, 10 (15), No. e019671.

(4) Fayaz Farkhad, B.; Karan, A.; Albarracín, D. Longitudinal Pathways to Influenza Vaccination Vary With Socio-Structural Disadvantages. *Ann. Behav. Med.* **2022**, 56 (5), 472−483.

(5) Vashist, K.; Choi, D.; Patel, S. A. Identification of groups at high risk for under-coverage of seasonal influenza vaccination: A national study to inform vaccination priorities during the COVID-19 pandemic. *Ann. Epidemiol.* **2022**, 68, 16−23.

(6) Dobson, J.; Whitley, R. J.; Pocock, S.; Monto, A. S. Oseltamivir treatment for influenza in adults: a meta-analysis of randomised controlled trials. *Lancet* **2015**, 385 (9979), 1729−1737.

(7) Doshi, P.; Heneghan, C.; Jefferson, T. Oseltamivir for influenza. *Lancet* **2016**, 387 (10014), 124.

(8) Kumar, S.; Goicoechea, S.; Kumar, S.; Pearce, C. M.; Durvasula, R.; Kempaiah, P.; Rathi, B.; Poonam. Oseltamivir analogs with potent anti-influenza virus activity. *Drug Discovery Today* **2020**, 25 (8), 1389−1402.

(9) Mattila, J. M.; Vuorinen, T.; Waris, M.; Antikainen, P.; Heikkinen, T. Oseltamivir treatment of influenza A and B infections

in infants. *Influenza and Other Respiratory Viruses* **2021**, *15* (5), 618–624.

(10) MacLaren, R.; Francisco, J.; Fetters, M.; Brady, J.; Kim, C.; Welker, C. Oseltamivir-Associated Bradycardia in Critically Ill Patients. *Ann. Pharmacother.* **2021**, *55* (11), 1318–1325.

(11) Wang-Jairaj, J.; Miller, I.; Joshi, A.; Jayabalan, T.; Peppercorn, A.; Zammit-Tabona, P.; Oliver, A. Zanamivir aqueous solution in severe influenza: A global Compassionate Use Program, 2009–2019. *Influenza and Other Respiratory Viruses* **2022**, *16* (3), 542–551.

(12) Alame, M. M.; Massaad, E.; Zaraket, H. Peramivir: A Novel Intravenous Neuraminidase Inhibitor for Treatment of Acute Influenza Infections. *Front. Microbiol.* **2016**, *7*, 7–450.

(13) Fang, Y. H.; Hsu, T. H.; Lin, T. Y.; Liu, C. H.; Chou, S. C.; Wu, J. Y.; Perng, P. C. Comparing intravenous peramivir with oral oseltamivir for patients with influenza: a meta-analysis of randomized controlled trials. *Expert Rev. Anti-Infect. Ther.* **2021**, *19* (8), 1039–1046.

(14) McLaughlin, M. M.; Skoglund, E. W.; Ison, M. G. Peramivir: an intravenous neuraminidase inhibitor. *Expert Opin. Pharmacother.* **2015**, *16* (12), 1889–1900.

(15) Shetty, A. K.; Wester, A. Peramivir injection in the treatment of acute influenza: a review of the literature. *Infect. Drug Resist.* **2016**, *9*, 201–214.

(16) Higashiguchi, M.; Matsumoto, T.; Fujii, T. A meta-analysis of laninamivir octanoate for treatment and prophylaxis of influenza. *Antivir. Ther.* **2018**, *23* (2), 157–165.

(17) Nakano, T.; Yamaguchi, H.; Chiba, T.; Shiosakai, K.; Chikada, S.; Matsuoka, Y. The safety and efficacy of the long-acting neuraminidase inhibitor laninamivir octanoate hydrate for Inhalation Suspension Set in children under the age of 5 in a post-marketing surveillance. *J. Infect. Chemother.* **2021**, *27* (10), 1436–1446.

(18) Palomba, E.; Castelli, V.; Renisi, G.; Bandera, A.; Lombardi, A.; Gori, A. Antiviral Treatments for Influenza. *Semin. Respir. Crit. Care Med.* **2021**, *42* (06), 859–872.

(19) Meijer, A.; Rebelo-de-Andrade, H.; Correia, V.; Besselaar, T.; Drager-Dayal, R.; Fry, A.; Gregory, V.; Gubareva, L.; Kageyama, T.; Lackenby, A.; et al. Global update on the susceptibility of human influenza viruses to neuraminidase inhibitors, 2012–2013. *Antiviral Res.* **2014**, *110*, 31–41.

(20) Aledavood, E.; Selmi, B.; Estarellas, C.; Masetti, M.; Luque, F. J. From Acid Activation Mechanisms of Proton Conduction to Design of Inhibitors of the M2 Proton Channel of Influenza A Virus. *Front. Mol. Biosci.* **2022**, *8*, 796229.

(21) Alves Galvão, M. G.; Rocha Crispino Santos, M. A.; Alves da Cunha, A. J. Amantadine and rimantadine for influenza A in children and the elderly. *Cochrane Database Syst. Rev.* **2014**, *2014* (11), CD002745.

(22) Pahwa, R. Amantadine: an old drug reborn. *Lancet Neurol.* **2021**, *20* (12), 975–977.

(23) Lamb, R. A. The Structure, Function, and Pathobiology of the Influenza A and B Virus Ion Channels. *Cold Spring Harbor Perspect. Med.* **2020**, *10* (11), a038505.

(24) Caceres, C. J.; Seibert, B.; Cargnin Faccin, F.; Cardenas-Garcia, S.; Rajao, D. S.; Perez, D. R. Influenza antivirals and animal models. *FEBS Open Bio* **2022**, *12* (6), 1142–1165.

(25) Hirotsu, N.; Sakaguchi, H.; Fukao, K.; Kojima, S.; Piedra, P. A.; Tsuchiya, K.; Uehara, T. Baloxavir safety and clinical and virologic outcomes in influenza virus-infected pediatric patients by age group: age-based pooled analysis of two pediatric studies conducted in Japan. *BMC Pediatr.* **2023**, *23* (1), 35.

(26) Kausar, S.; Said Khan, F.; Ishaq Mujeeb, Ur R. M.; Akram, M.; Riaz, M.; Rasool, G.; Hamid Khan, A.; Saleem, I.; Shamim, S.; Malik, A. A review: Mechanism of action of antiviral drugs. *Int. J. Immunopathol. Pharmacol.* **2021**, *35*, 20587384211002621.

(27) Berezin, V.; Bogoyavlenskiy, A.; Alexyuk, M.; Alexyuk, P. Plant Metabolites as Antiviral Preparations Against Coronaviruses. *J. Med. Food.* **2021**, *24* (10), 1028–1038.

(28) Gomes, P. W. P.; Martins, L.; Gomes, E.; Muribeca, A.; Pamplona, S.; Komesu, A.; Bichara, C.; Rai, M.; Silva, C.; Silva, M.

Antiviral Plants from Marajó Island, Brazilian Amazon: A Narrative Review. *Molecules* **2022**, *27* (5), 1542.

(29) Mammari, N.; Krier, Y.; Albert, Q.; Devocelle, M.; Varbanov, M. Plant-Derived Antimicrobial Peptides as Potential Antiviral Agents in Systemic Viral Infections. *Pharmaceuticals* **2021**, *14* (8), 774.

(30) Corcoran, M. P.; McKay, D. L.; Blumberg, J. B. Flavonoid Basics: Chemistry, Sources, Mechanisms of Action, and Safety. *J. Nutr. Gerontol. Geriatr.* **2012**, *31*, 176–189.

(31) Mennen, L. I.; Walker, R.; Bennetau-Pelissero, C.; Scalbert, A. Risks and safety of polyphenol consumption. *Am. J. Clin. Nutr.* **2005**, *81*, 326S.

(32) Chen, M.; Hu, D.; Li, X.; Yang, S.; Zhang, W.; Li, P.; Song, B. Antiviral activity and interaction mechanisms study of novel glucopyranoside derivatives. *Bioorg. Med. Chem. Lett.* **2015**, *25*, 3840–3844.

(33) Al-Karmalawy, A. A.; Farid, M. M.; Mostafa, A.; Ragheb, A. Y.; H Mahmoud, S.; Shehata, M.; Shama, N. M. A.; GabAllah, M.; Mostafa-Hedeab, G.; Marzouk, M. M. Naturally Available Flavonoid Aglycones as Potential Antiviral Drug Candidates against SARS-CoV-2. *Molecules* **2021**, *26* (21), 6559.

(34) Badshah, S. L.; Faisal, S.; Muhammad, A.; Poulson, B. G.; Emwas, A. H.; Jaremko, M. Antiviral activities of flavonoids. *Biomed. Pharmacother.* **2021**, *140*, 111596.

(35) Di Petrillo, A.; Orrù, G.; Fais, A.; Fantini, M. C. Quercetin and its derivates as antiviral potentials: A comprehensive review. *Phytother. Res.* **2022**, *36* (1), 266–278.

(36) Sheridan, R.; Spelman, K. Polyphenolic promiscuity, inflammation-coupled selectivity: Whether PAINs filters mask an antiviral asset. *Front. Pharmacol* **2022**, *13*, 909945.

(37) Shorobi, F. M.; Nisa, F. Y.; Saha, S.; Chowdhury, M. A. H.; Srisuphanunt, M.; Hossain, K. H.; Rahman, M. A. Quercetin: A Functional Food-Flavonoid Incredibly Attenuates Emerging and Re-Emerging Viral Infections through Immunomodulatory Actions. *Molecules* **2023**, *28* (3), 938.

(38) Kaul, R.; Paul, P.; Kumar, S.; Büsselberg, D.; Dwivedi, V. D.; Chaari, A. Promising Antiviral Activities of Natural Flavonoids against SARS-CoV-2 Targets: Systematic Review. *Int. J. Mol. Sci.* **2021**, *22* (20), 11069.

(39) Khazeei Tabari, M. A.; Iranpanah, A.; Bahramsoltani, R.; Rahimi, R. Flavonoids as Promising Antiviral Agents against SARS-CoV-2 Infection: A Mechanistic Review. *Molecules* **2021**, *26* (13), 3900.

(40) Zhan, Y.; Ta, W.; Tang, W.; Hua, R.; Wang, J.; Wang, C.; Lu, W. Potential antiviral activity of isorhamnetin against SARS-CoV-2 spike pseudotyped virus in vitro. *Drug Dev. Res.* **2021**, *82* (8), 1124–1130.

(41) Dayem, A. A.; Choi, H. Y.; Kim, Y. B.; Cho, S. G. Antiviral effect of methylated flavonol isorhamnetin against influenza. *PLoS One* **2015**, *10* (3), No. e0121610.

(42) Gong, G.; Guan, Y. Y.; Zhang, Z. L.; Rahman, K.; Wang, S. J.; Zhou, S.; Luan, X.; Zhang, H. Isorhamnetin: A review of pharmacological effects. *Biomed. Pharmacother.* **2020**, *128*, 110301.

(43) Li, J.; Xu, Y.; Lin, Z.; Guan, L.; Chen, S.; Zhou, L. Isorhamnetin inhibits amplification of influenza A H1N1 virus inflammation mediated by interferon via the RIG-I/JNK pathway. *Ann. Transl. Med.* **2021**, *9* (16), 1327.

(44) Kwofie, S. K.; Broni, E.; Asiedu, S. O.; Kwarko, G. B.; Dankwa, B.; Enninful, K. S.; Tiburu, E. K.; Wilson, M. D. Cheminformatics-Based Identification of Potential Novel Anti-SARS-CoV-2 Natural Compounds of African Origin. *Molecules* **2021**, *26* (2), 406.

(45) Nakamura, S.; Fujimoto, K.; Matsumoto, T.; Ohta, T.; Ogawa, K.; Tamura, H.; Matsuda, H.; Yoshikawa, M. Structures of acylated sucroses and an acylated flavonol glycoside and inhibitory effects of constituents on aldose reductase from the flower buds of Prunus mume. *J. Nat. Med.* **2013**, *67*, 799–806.

(46) Yanze, L.; Yangjie, W.; Ke, Y.; et al. New galloylated flavonoidal glycoside and gallotannins from the leaves of loropetalum chinense oliv. *Nat. Prod. Res. Dev.* **1997**, *9*, 12.

(47) He, H. F. Recognition of Gallotannins and the Physiological Activities: From Chemical View. *Front. Nutr.* **2022**, *9*, 888892.

(48) Romani, A.; Pinelli, P.; Galardi, C.; Mulinacci, N.; Tattini, M. Identification and quantification of galloyl derivatives, flavonoid glycosides and anthocyanins in leaves of Pistacia lentiscus L. *Phytochem. Anal.* **2002**, *13* (2), 79−86.

(49) Liu, Y.; Fernie, A. R.; Tohge, T. Diversification of Chemical Structures of Methoxylated Flavonoids and Genes Encoding Flavonoid-O-Methyltransferases. *Plants* **2022**, *11* (4), 564.

(50) Graefe, E. U.; Wittig, J.; Mueller, S.; Riethling, A.; Uehleke, B.; Drewelow, B.; Pforte, H.; Jacobasch, G.; Derendorf, H.; Veit, M. Pharmacokinetics and bioavailability of quercetin glycosides in humans. *J. Clin. Pharmacol.* **2001**, *41*, 492−499.

(51) Karas, D.; Ulrichova, J.; Valentova, K. Galloylation of polyphenols alters their biological activity. *Food Chem. Toxicol.* **2017**, *105*, 223−240.

(52) Menezes, J. C.; Orlikova, B.; Morceau, F.; Diederich, M. Natural and Synthetic Flavonoids: Structure-Activity Relationship and Chemotherapeutic Potential for the Treatment of Leukemia. *Crit. Rev. Food Sci. Nutr.* **2016**, *56* (sup1), S4−S28.

(53) Scotti, L.; Bezerra Mendonca Junior, F. J.; Magalhaes Moreira, D. R.; da Silva, M. S.; Pitta, I. R.; Scotti, M. T. SAR, QSAR and Docking of Anticancer Flavonoids and Variants: A Review. *Curr. Top. Med. Chem.* **2012**, *12*, 2785−2809.

(54) Yang, Z. F.; Bai, L. P.; Huang, W. B.; Li, X. Z.; Zhao, S. S.; Zhong, N. S.; Jiang, Z. H. Comparison of in vitro antiviral activity of tea polyphenols against influenza A and B viruses and structure-activity relationship analysis. *Fitoterapia* **2014**, *93*, 47−53.

(55) Kajiya, K.; Hojo, H.; Suzuki, M.; Nanjo, F.; Kumazawa, S.; Nakayama, T. Relationship between antibacterial activity of (+)-catechin derivatives and their interaction with a model membrane. *J. Agric. Food Chem.* **2004**, *52* (6), 1514−1519.

(56) Copmans, D.; Orellana-Paucar, A. M.; Steurs, G.; Zhang, Y.; Ny, A.; Foubert, K.; Exarchou, V.; Siekierska, A.; Kim, Y.; De Borggraeve, W.; Dehaen, W.; Pieters, L.; de Witte, P. A. M. Methylated flavonoids as anti-seizure agents: Naringenin 4',7-dimethyl ether attenuates epileptic seizures in zebrafish and mouse models. *Neurochem. Int.* **2018**, *112*, 124−133.

(57) Koirala, N.; Thuan, N. H.; Ghimire, G. P.; Thang, D. V.; Sohng, J. K. Methylation of flavonoids: Chemical structures, bioactivities, progress and perspectives for biotechnological production. *Enzyme Microb. Technol.* **2016**, *86*, 103−116.

(58) Uchiyama, H.; Kadota, K.; Nakanishi, A.; Tandia, M.; Tozuka, Y. A simple blending with α-glycosylated naringin produces enhanced solubility and absorption of pranlukast hemihydrate. *Int. J. Pharm.* **2019**, *567*, 118490.

(59) Morand, C.; Manach, C.; Crespy, V.; Remesy, C. Respective bioavailability of quercetin aglycone and its glycosides in a rat model. *Biofactors* **2000**, *12* (1−4), 169−174.

(60) Choudhury, R.; Chowrimootoo, G.; Srai, K.; Debnam, E.; Rice-Evans, C. A. Interactions of the flavonoid naringenin in the gastrointestinal tract and the influence of glycosylation. *Biochem. Biophys. Res. Commun.* **1999**, *265* (2), 410−415.

(61) Indrayanto, G.; Putra, G.; Suhud, F. Chapter Six—Validation of in-vitro bioassay methods: Application in herbal drug research. *Profiles of Drug Substances, Excipients and Related Methodology*; Al-Majed, A. A., Ed.; Academic Press, Vol. 46, 2021; pp 273−307.

(62) Weerapreeyakul, N.; Nonpunya, A.; Barusrux, S.; Thitimetharoch, T.; Sripanidkulchai, B. Evaluation of the anticancer potential of six herbs against a hepatoma cell line. *Chin. Med.* **2012**, *7* (1), 15.

(63) Klimov, A.; Balish, A.; Veguilla, V.; Sun, H.; Schiffer, J.; Lu, X.; Katz, J. M.; Hancock, K. Influenza virus titration, antigenic characterization, and serological methods for antibody detection. *Methods Mol. Biol.* **2012**, *865*, 25−51.

(64) Reed, L. J.; Muench, H. A simple method of estimating fifty per cent endpoints. *Am. J. Epidemiol.* **1938**, *27*, 493−497.

(65) Berdimuratova, G. D.; Muzychkina, R. A.; Korulkin, D. Y.; Abilov, Z. A. Tulegenova AU Bioactive constituents of plants. *Extraction, Separation and Analysis*: Atamura, Almaty, 2006; p 307.

(66) Berridge, M. V.; Tan, A. S. Characterization of the cellular reduction of 3-(4,5-dimethylthiazol-2-yl)-2,5-diphenyltetrazolium bromide (MTT): subcellular localization, substrate dependence, and involvement of mitochondrial electron transport in MTT reduction. *Arch. Biochem. Biophys.* **1993**, *303* (2), 474−482.

(67) Turmagambetova, A. S.; Sokolova, N. S.; Bogoyavlenskiy, A. P.; Berezin, V. E.; Lila, M. A.; Cheng, D. M.; Dushenkov, V. New functionally-enhanced soy proteins as food ingredients with anti-viral activity. *VirusDisease* **2015**, *26* (3), 123−132.

(68) Berezin, V.; Abdukhakimova, D.; Trenozhnikova, L.; Bogoyavlenskiy, A.; Turmagambetova, A.; Issanov, A.; Azizan, A. Antiviral activities of extremophilic actinomycetes extracts from Kazakhstan's unique ecosystems against influenza viruses and paramyxoviruses. *Virol. J.* **2019**, *16* (1), 150.

(69) Wang, J. X.; Zhou, J. Y.; Yang, Q. W.; Chen, Y.; Li, X.; Piao, Y. A.; Li, H. Y. An improved embryonated chicken egg model for the evaluation of antiviral drugs against influenza A virus. *J. Virol. Methods* **2008**, *153*, 218−222.

(70) Mohamed, K.; Yazdanpanah, N.; Saghazadeh, A.; Rezaei, N. Computational drug discovery and repurposing for the treatment of COVID-19: A systematic review. *Bioorg. Chem.* **2021**, *106*, 104490.

(71) Bogoyavlenskiy, A.; Alexyuk, M.; Alexyuk, P.; Berezin, V.; Almalki, F. A.; Ben Hadda, T.; Alqahtani, A. M.; Ahmed, S. A.; Dall'Acqua, S.; Jamalis, J. Computer Analysis of the Inhibition of ACE2 by Flavonoids and Identification of Their Potential Antiviral Pharmacophore Site. *Molecules* **2023**, *28* (9), 3766.

(72) Barber, R. D. Software to Visualize Proteins and Perform Structural Alignments. *Curr. Protoc.* **2021**, *1* (11), No. e292.

(73) Mooers, B. H. M.; Brown, M. E. Templates for writing PyMOL scripts. *Protein Sci.* **2021**, *30* (1), 262−269.

(74) Mooers, B. H. M. Shortcuts for faster image creation in PyMOL. *Protein Sci.* **2020**, *29* (1), 268−276.

(75) Goodsell, D. S.; Sanner, M. F.; Olson, A. J.; Forli, S. The AutoDock suite at 30. *Protein Sci.* **2021**, *30* (1), 31−43.

(76) Tang, S.; Chen, R.; Lin, M.; Lin, Q.; Zhu, Y.; Ding, J.; Hu, H.; Ling, M.; Wu, J. Accelerating AutoDock Vina with GPUs. *Molecules* **2022**, *27* (9), 3041.

(77) Lee, S. H.; Kim, B.; Oh, M. J.; Yoon, J.; Kim, H. Y.; Lee, K. J.; Lee, J. D.; Choi, K. Y. Persicaria hydropiper (L.) spach and its flavonoid components, isoquercitrin and isorhamnetin, activate the Wnt/β-catenin pathway and inhibit adipocyte differentiation of 3T3-L1 cells. *Phytother. Res.* **2011**, *25* (11), 1629−1635.

(78) Oh, H. M.; Kwon, B. M.; Baek, N. I.; Kim, S. H.; Chung, I. S.; Park, M. H.; Park, H. W.; Lee, J. H.; Park, H. W.; Kim, E. J.; Kim, D. K. Inhibitory activity of isorhamnetin from Persicaria thunbergii on Farnesyl Protein Transferase. *Arch. Pharmacal Res.* **2005**, *28* (2), 169−171.

(79) Tian, H.; Ketkar, R.; Tao, P. ADMETboost: a web server for accurate ADMET prediction. *J. Mol. Model.* **2022**, *28*, 408.

(80) Jia, C. Y.; Li, J. Y.; Hao, G. F.; Yang, G. F. A drug-likeness toolbox facilitates ADMET study in drug discovery. *Drug Discovery Today* **2020**, *25*, 248−258.

(81) Hasan, A. H.; Murugesan, S.; Amran, S. I.; Chander, S.; Alanazi, M. M.; Hadda, T. B.; Shakya, S.; Pratama, M. R. F.; Das, B.; Biswas, S.; Jamalis, J. Novel thiophene Chalcones-Coumarin as acetylcholinesterase inhibitors: Design, synthesis, biological evaluation, molecular docking, ADMET prediction and molecular dynamics simulation. *Bioorg. Chem.* **2022**, *119*, 105572.

(82) Berendsen, H. J. C.; van der Spoel, D.; van Drunen, R. GROMACS: A message-passing parallel molecular dynamics implementation. *Comput. Phys. Commun.* **1995**, *91* (1−3), 43−56.

(83) Abraham, M. J.; Murtola, T.; Schulz, R.; Páll, S.; Smith, J. C.; Hess, B.; Lindahl, E. GROMACS: High performance molecular simulations through multi-level parallelism from laptops to super-computers. *SoftwareX* **2015**, *1−2*, 19−25.

(84) Best, R. B.; Zhu, X.; Shim, J.; Lopes, P. E. M.; Mittal, J.; Feig, M.; MacKerell, A. D., Jr. Optimization of the Additive CHARMM All-Atom Protein Force Field Targeting Improved Sampling of the Backbone ϕ, ψ and Side-Chain $\chi 1$ and $\chi 2$ Dihedral Angles. *J. Chem. Theory Comput.* **2012**, *8* (9), 3257−3273.

(85) Lee, J.; Cheng, X.; Swails, J. M.; Yeom, M. S.; Eastman, P. K.; Lemkul, J. A.; Wei, S.; Buckner, J.; Jeong, J. C.; Qi, Y.; Jo, S.; Pande, V. S.; Case, D. A.; Brooks, C. L., III; MacKerell, A. D., Jr.; Klauda, J. B.; Im, W. CHARMM-GUI Input Generator for NAMD, GROMACS, AMBER, OpenMM, and CHARMM/OpenMM Simulations Using the CHARMM36 Additive Force Field. *J. Chem. Theory Comput.* **2016**, *12* (1), 405−413.

(86) Hasan, A. H.; Abdulrahman, F. A.; Obaidullah, A. J.; Alotaibi, H. F.; Alanazi, M. M.; Noamaan, M. A.; Murugesan, S.; Amran, S. I.; Bhat, A. R.; Jamalis, J. Discovery of Novel Coumarin-Schiff Base Hybrids as Potential Acetylcholinesterase Inhibitors: Design, Synthesis, Enzyme Inhibition, and Computational Studies. *Pharmaceuticals* **2023**, *16* (7), 971.

(87) Abdalla Ali, A.; Mhamad, S. A.; Hasan, A. H.; Ahmad, I.; Abdullah, S. A.; Jamil, S.; Patel, H.; Murugesan, S.; Jamalis, J. Synthesis, biological evaluation and molecular modeling studies of modulated benzyloxychalcones as potential acetylcholinesterase inhibitors. *J. Biomol. Struct. Dyn.* **2023**, 1−12 (published online).

(88) Nosé, S.; Klein, M. L. Constant pressure molecular dynamics for molecular systems. *Mol. Phys.* **1983**, *50* (5), 1055−1076.

(89) Grest, G. S.; Kremer, K. Molecular dynamics simulation for polymers in the presence of a heat bath. *Phys. Rev. A* **1986**, *33* (5), 3628−3631.

(90) Humphrey, W.; Dalke, A.; Schulten, K. VMD: Visual molecular dynamics. *J. Mol. Graphics* **1996**, *14* (1), 33−38.

(91) Salih, R. H. H.; Hasan, A. H.; Hussein, A. J.; Samad, M. K.; Shakya, S.; Jamalis, J.; Hawaiz, F. E.; Pratama, M. R. F. One-pot synthesis, molecular docking, ADMET, and DFT studies of novel pyrazolines as promising SARS-CoV-2 main protease inhibitors. *Res. Chem. Intermed.* **2022**, *48*, 4729−4751.

(92) Essmann, U.; Perera, L.; Berkowitz, M. L.; Darden, T.; Lee, H.; Pedersen, L. G. A smooth particle mesh Ewald method. *J. Chem. Phys.* **1995**, *103* (19), 8577−8593.

(93) Valdés-Tresanco, M. S.; Valdés-Tresanco, M. E.; Valiente, P. A.; Moreno, E. gmx_MMPBSA: A New Tool to Perform End-State Free Energy Calculations with GROMACS. *J. Chem. Theory Comput.* **2021**, *17* (10), 6281−6291.

(94) Mirzaei, S.; Eisvand, F.; Hadizadeh, F.; Mosaffa, F.; Ghasemi, A.; Ghodsi, R. Design, synthesis and biological evaluation of novel 5,6,7-trimethoxy-N-aryl-2-styrylquinolin-4-amines as potential anticancer agents and tubulin polymerization inhibitors. *Bioorg. Chem.* **2020**, *98*, 103711.

(95) Hasan, A. H.; Shakya, S.; Hussain, F. H. S.; Murugesan, S.; Chander, S.; Pratama, M. R. F.; Jamil, S.; Das, B.; Biswas, S.; Jamalis, J. Design, synthesis, anti-acetylcholinesterase evaluation and molecular modelling studies of novel coumarin-chalcone hybrids. *J. Biomol. Struct. Dyn.* **2023**, *41*, 11450−11462.

(96) Kumari, R.; Kumar, R.; Lynn, A. g_mmpbsa-A GROMACS Tool for High-Throughput MM-PBSA Calculations. *J. Chem. Inf. Model.* **2014**, *54* (7), 1951−1962.

(97) Pronk, S.; Páll, S.; Schulz, R.; Larsson, P.; Bjelkmar, P.; Apostolov, R.; Shirts, M. R.; Smith, J. C.; Kasson, P. M.; van der Spoel, D.; Hess, B.; Lindahl, E. GROMACS 4.5: a high-throughput and highly parallel open source molecular simulation toolkit. *Bioinformatics* **2013**, *29* (7), 845−854.

(98) Machaba, K. E.; Mhlongo, N. N.; Soliman, M. E. S. Induced Mutation Proves a Potential Target for TB Therapy: A Molecular Dynamics Study on LprG. *Cell Biochem. Biophys.* **2018**, *76* (3), 345−356.